Fordham, D., Brown, S., Wigley, T., Rahbek, C., 2019. Cradles of diversity: unlikely relics of regional climate stability. Current Biology (in press).

Extended Methods

Continuous paleoclimate simulations of gridded monthly-mean temperature at the surface (TS) for the period 21,000 BP to 100 BP were accessed from the TRaCE21ka experiment [1] using PaleoView [2]. Multi-century pre-industrial control runs of annual-mean TS for 18 different AOGCMs (Table 1) were retrieved from the Coupled Model Intercomparison Project Phase 5 [3] and resampled to a common 2.5° x 2.5° grid using bilinear interpolation. Bilinear interpolation was chosen because (i) the source and destination grids were rectilinear, (ii) temperature varies smoothly spatially, and (iii) bilinear interpolation reasonably retains the integrity and limitations of the original model output data, where orography is highly smoothed relative to the real-world [4].

Pre-industrial control runs are multi-century unforced climate simulations, where the initial model conditions are set based on atmospheric gas concentrations pre-wide-scale industrialisation (c. 1750 – 1850 CE), combined with non-evolving boundary conditions [3]. We elected to use only the first realisation (r1i1p1) from each AOGCM for the pre-industrial control runs because all models, with the exception of the Community Climate System Model ver. 4 (CCSM4) [5], only had a single realisation for pre-industrial control conditions. Furthermore, the additional pre-industrial realisations (r2i1p1 and r3i1p1) for the CCSM4 model ran for considerably shorter periods: 156 and 120 years (Table 1). These pre-industrial control runs were used as a baseline for determining centuries of large changes in global-mean temperature (see below).

Identifying 'extreme' natural periods of global climate change.

We used multi-century pre-industrial control runs from the AOGCMs to estimate internally-generated natural variability in area-weighted global-mean trend magnitudes in TS(°C/year) [6] using generalised least squares (GLS) regression and maximally (1-year) overlapping windows i.e., a 100-year moving window with a 1-year step between windows. GLS regression models were generated using the *nlme* package for R [7]. Trends for the 18 AOGCMs were calculated using area-weighted global-mean temperatures based on the slope of the GLS model. An AR(1) error structure was chosen to minimise any effect of temporal auto-correlation in the model residuals [7]. The resulting global pre-industrial model trends (i.e., the slope of the regression against time) for TS were used to generate a multi-model empirical cumulative distribution function (CDF) using unsigned (i.e. absolute) trends (Figure 1). Because the number of years varied between pre-industrial control runs from different AOGCMs (Table 1) we used a bootstrap procedure to ensure that all models had equal weights in the CDF. This involved randomly selecting 141 centuries from each model (with replacement) — 141 is the minimum number of maximally overlapping century-length windows across all models. The bootstrap procedure was repeated 1000 times. Centuries having extreme trends were defined as those where the trend exceeded the 90th percentile of the multi-model control-run CDF. The 90th percentile is commonly used in climate change research to identify extreme events [8, 9].

We used a similar approach to calculate paleoclimate trend magnitudes in annual TS (using the TraCE-21ka daily paleoclimate simulations) using maximally overlapping century "windows" spanning the period from 21,000 BP to 100 BP. The primary difference being that for the paleoclimate simulations we calculated 'local' measures of trend in annual mean surface temperature for each grid-cell (n = 10,368 cells) as well as the area-weighted global-mean trend magnitude (see Figure 2 for a schematic of the workflow). We also calculated grid-cell estimates of variability, where variability was defined as the standard deviation (SD) of the residuals about the local trend [10]. We did not bootstrap the paleoclimate data because we only had one model.

We applied the 90th percentile trend threshold of the multi-model control-run CDF to the time series of area-weighted global-mean paleoclimate trends (based on maximal overlapping windows) to identify specific centuries of extreme change in global-mean temperature during the period 21,000 BP to 100 BP. We then subset the time series of paleoclimate simulations based on these periods of extreme change in area-weighted global-mean temperature. In doing so, 'local' measures of trend and variability (i.e., at the grid cell) were constrained to centuries of unusually high trends in global-mean temperature.

To check that our definition of extreme centuries of change in global-mean temperature was appropriate, we determined the amount of time a millennium was considered 'extreme'. We did this by calculating the % of time that a millennium was characterised by trends $\geq 90^{th}$ percentile of the control run trends (Figure 3). This confirmed that known large-scale climatic events during the last deglaciation (e.g. Bølling–Allerød, Younger Dryas, Holocene climate optimum etc.) were correctly identified as periods of extreme climate change in our analysis. We also examined the trend in global-mean temperature through time (Figure 3).

Mapping past climate stability

We calculated the median values of the century trends and variability about the trends for each grid cell for the periods of rapid change in global-mean temperature from 21,000 BP to 100 BP. We then mapped cells along a gradient of climate stability for land and ocean realms separately. The use of both trend and variability combines information about low frequency (trend) and high frequency (SD) variability. We classified cells according to eight levels of climate stability, ranging from 'extremely stable' to 'extremely unstable': (i) $\leq 10^{th}$ percentile of both trend and variability; (ii) $> 10^{th}$ and $\leq 25^{th}$ percentile of both trend and variability; (iii) $> 25^{th}$ and $\leq 50^{th}$ percentile of both trend and variability; (iv) $\leq 50^{th}$ percentile of trend and $\geq 50^{th}$ percentile of variability; (v) $\geq 50^{th}$ percentile of trend and $\leq 50^{th}$ percentile of variability; (vi) $\geq 50^{th}$ and $< 75^{th}$ percentile of both trend and variability; (vii) $\geq 75^{th}$ and $< 90^{th}$ percentile of both trend and variability; (viii) $\geq 90^{th}$ percentile of both trend and variability.

To test whether climate-related refugia are likely to have been stationary in time and space during the most recent deglaciation event, we calculated and mapped the percentage of time each grid cell was characterised by 'stable' and 'extremely stable' climatic conditions in the face of unusually high trends in global mean temperatures. If a window is centred on, say, year N, then we used the 4066 land and 6302 ocean gridded values of trend magnitude and SD to calculate the distributions of these data corresponding to this year, and determine the 10th and 25th percentile points for land and ocean biomes separately. For any given grid point, the climate was defined as 'stable' if both the trend magnitude and SD were $\leq$ the 25th percentile, and as 'extremely stable' if both were $\leq$ the 10th percentile. At any grid point then, for the 'stable' case, if 1 denotes stable and 0 denotes not stable, we have a time series of 0s and 1s that identify periods of stable climate. We calculated time spent in 'extremely stable' climate conditions in a similar way. We chose the 10th and 25th percentiles because they are commonly used in climate change research to identify extreme events [9, 11]. However, there is no way of knowing with any certainty whether these thresholds relate directly to mechanisms responsible for spatiotemporal variation in biodiversity patterns. To determine how sensitive our results are to the choice of threshold we did a sensitivity analysis, whereby we varied the thresholds for stable and extremely stable climates ± 10% (n = 20 stratified samples), calculated the grid cell SD and mapped these values.

References

1. Liu, Z., Otto-Bliesner, B.L., He, F., Brady, E.C., Tomas, R., Clark, P.U., Carlson, A.E., Lynch-Stieglitz, J., Curry, W., Brook, E., et al. (2009). Transient Simulation of Last Deglaciation with a New Mechanism for Bølling-Allerød Warming. Science *325*, 310-314.
2. Fordham, D.A., Saltré, F., Haythorne, S., Wigley, T.M.L., Otto-Bliesner, B.L., Chan, K., and Brook, B.W. (2017). PaleoView: A tool for generating continuous climate projections spanning the last 21,000 years at regional and global scales Ecography *40*, 1348-1358.
3. Taylor, K.E., Stouffer, R.J., and Meehl, G.A. (2011). An Overview of CMIP5 and the Experiment Design. Bulletin of the American Meteorological Society *93*, 485-498.
4. Fordham, D.A., Saltre, F., Haythorne, S., Wigley, T.M.L., Otto-Bliesner, B.L., Chan, K.C., and Brook, B.W. (2017). PaleoView: a tool for generating continuous climate projections spanning the last 21 000 years at regional and global scales. Ecography *40*, 1348-1358.
5. Gent, P.R., Danabasoglu, G., Donner, L.J., Holland, M.M., Hunke, E.C., Jayne, S.R., Lawrence, D.M., Neale, R.B., Rasch, P.J., Vertenstein, M., et al. (2011). The Community Climate System Model Version 4. Journal of Climate *24*, 4973-4991.
6. Sen Gupta, A., Jourdain, N.C., Brown, J.N., and Monselesan, D. (2013). Climate Drift in the CMIP5 Models. Journal of Climate *26*, 8597-8615.
7. Pinheiro J, Bates D, DebRoy S, Sarkar D, and R Core Team (2017). nlme: Linear and Nonliner Mixed Effects Models. R package version 3.1-131 Edition, Pinheiro J, Bates D, DebRoy S, Sarkar D and R.C. Team, eds.
8. Harris, R.M.B., Beaumont, L.J., Vance, T.R., Tozer, C.R., Remenyi, T.A., Perkins-Kirkpatrick, S.E., Mitchell, P.J., Nicotra, A.B., McGregor, S., Andrew, N.R., et al. (2018). Biological responses to the press and pulse of climate trends and extreme events. Nature Climate Change *8*, 579-587.
9. Zhang, X., Alexander, L., Hegerl, G.C., Jones, P., Tank, A.K., Peterson, T.C., Trewin, B., and Zwiers, F.W. (2011). Indices for monitoring changes in extremes based on daily temperature and precipitation data. WIREs Clim Change *2*, 851-870.
10. Nadeau, C.P., Urban, M.C., and Bridle, J.R. (2017). Coarse climate change projections for species living in a fine-scaled world. Glob Chang Biol *23*, 12-24.
11. Hao, Z., AghaKouchak, A., and Phillips, T.J. (2013). Changes in concurrent monthly precipitation and temperature extremes. Environmental Research Letters *8*, 034014.
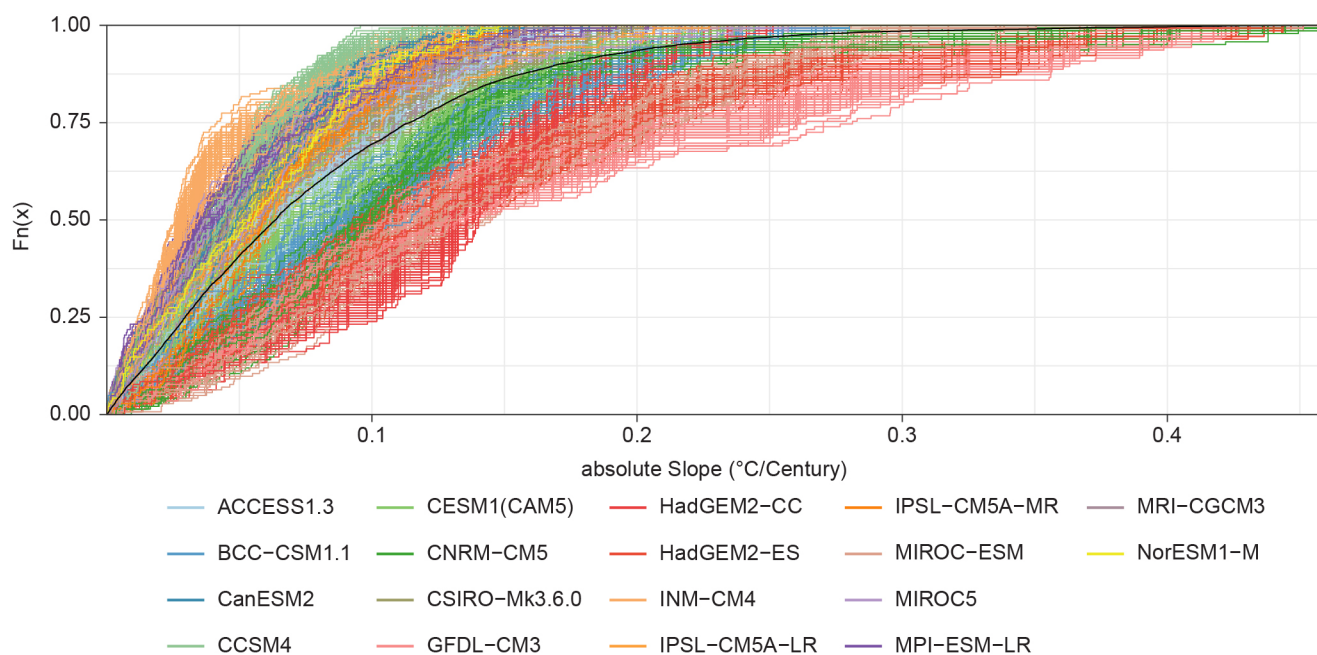
Figure 1: Cumulative Distribution Functions (CDFs) of trends in global-mean temperature for the pre-industrial CMIP5 control runs. Different colours represent the bootstrap replicates for each of the different models; the black line represents the mean of all the CDFs for each model bootstrap. Trends were calculated using a 100-year moving window with a 1-year step between windows.
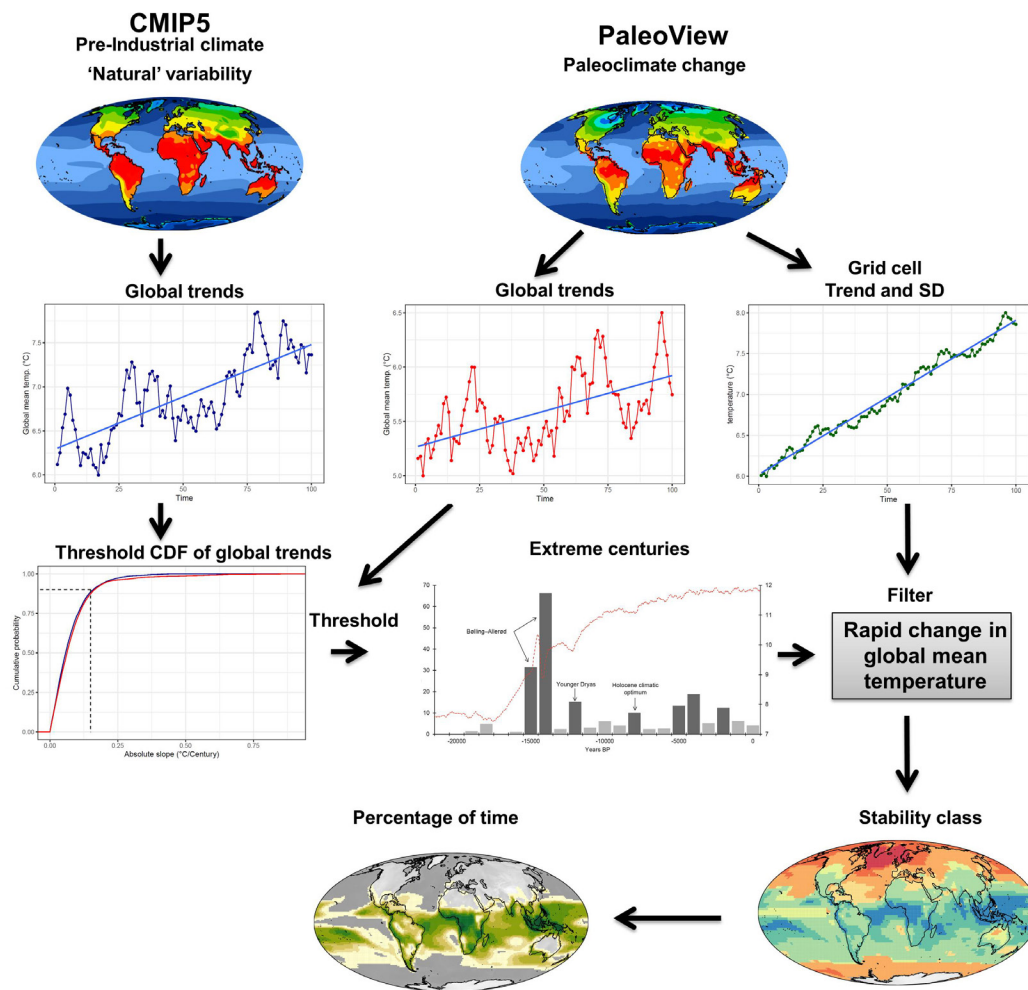
Figure 2: Workflow for estimating percentage of time spent in stable and extremely stable climates. CMIP5 pre-industrial control runs were used to estimate century trends in annual global mean temperature under conditions of natural variability focused on 100BP (1850 AD). The 90th percentile was used to calculate a threshold for identifying the most extreme century trends in global mean temperature for pre-industrial control runs. Century trends in annual global mean temperature and century trends and SD in annual grid cell mean temperature were generated for the last 21,000 using data from PaleoView. The threshold (90th percentile) for extreme century trends in global mean temperature for pre-industrial control runs was applied to the PaleoView estimates to identify centuries of rapid change (extreme centuries) in the past. These centuries were used to filter the time series of paleoclimate simulations of grid cell trends and SD, such that for each century of rapid change in global mean temperature, classes of climate stability were derived and the percentage of time a grid cell spent in a given stability class was calculated for all extreme centuries.
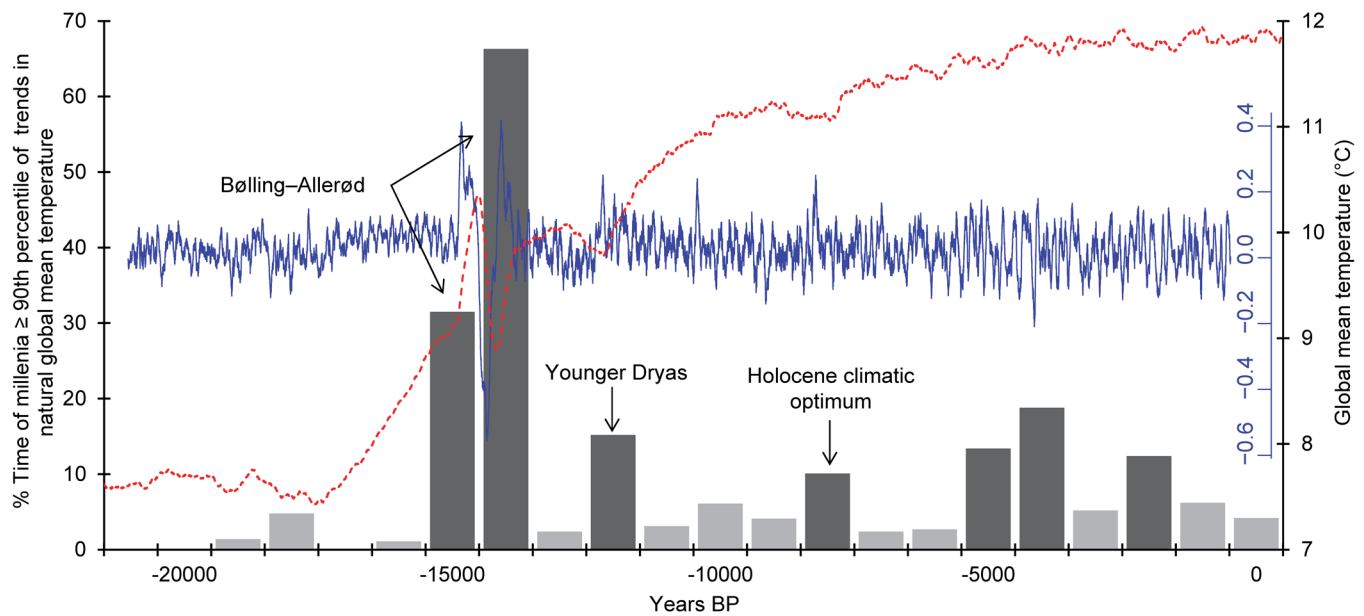
Figure 3: Percentage of time spent in 'extreme' conditions of global climate change defined as having century timescale trend magnitudes ≥ 90th percentile of the bootstrapped pre-industrial control-run trend magnitudes in global-mean temperature. The primary Y-axis and the vertical bars show the amount of time in a given millennium (X-axis) when the trend in global mean temperature is ≥ the cut-off threshold. Darker bars show millennia where centuries of unusually high trends in global mean temperatures occurred in > 10% of the millennia. The secondary (right hand) Y-axis and the dashed red line shows the global-mean temperature from the TraCE-21ka dataset (°C). The blue line shows the slope for the linear trend for the global-mean temperature from the TraCE-21ka dataset (°C per year). Major climatic events are shown with arrows.

Table S1: The <u>18 models used for the analysis of 'natural' trends under the pre-industrial control runs</u>

Model	Institution/s	Atmospheric Resolution (°)		Number of years[†]
		Lat	Long	
ACCESS 1.3	Commonwealth Scientific and Industrial Research Organisation / Bureau of Meteorology	1.9	1.2	500
BCC-CSM1.1	Beijing Climate Center, China Meteorological Administration	2.8	2.8	500
CanESM2	Canadian Centre for Climate Modelling and Analysis	2.8	2.8	996
CCSM4	National Center for Atmospheric Research	0.9	1.3	1,051
CESM1(CAM5)	National Center for Atmospheric Research	0.9	1.3	320
CNRM-CM5	Centre National de Recherches Meteorologiques / Centre Europeen de Recherche et Formation Avancees en Calcul Scientifique	1.4	1.4	850
CSIRO-Mk3.6.0	Commonwealth Scientific and Industrial Research Organisation / Queensland Climate Change Centre of Excellence	1.9	1.9	500
GFDL-CM3	National Oceanic and Atmospheric Administration Office of Oceanic and Atmospheric Research - Geophysical Fluid Dynamics Laboratory	2.0	2.5	500
HadGEM2-CC	Met Office Hadley Centre	1.3	1.9	240
HadGEM2-ES	Met Office Hadley Centre	1.3	1.9	575
INM-CM4	Institute for Numerical Mathematics	1.5	2.0	500
IPSL-CM5A-LR	Institut Pierre-Simon Laplace	1.9	3.8	1,000
IPSL-CM5A-MR	Institut Pierre-Simon Laplace	1.3	2.5	300
MIROC5	Atmosphere and Ocean Research Institute (The University of Tokyo), National Institute for Environmental Studies / Japan Agency for Marine-Earth Science and Technology	1.4	1.4	670
MIROC-ESM	Japan Agency for Marine-Earth Science and Technology, Atmosphere and Ocean Research Institute (The University of Tokyo) / National Institute for Environmental Studies	2.8	2.8	630
MPI-ESM-LR	Max Planck Institute for Meteorology	1.9	1.9	1,000
MRI-CGCM3	Meteorological Research Institute	1.1	1.1	500
NorESM1-M	Norwegian Climate Centre	1.9	2.5	501